PAPER

Check for updates

Thermal degradation of mango (*Mangifera indica*) wood sawdust in a nitrogen environment: characterization, kinetics, reaction mechanism, and thermodynamic analysis

Ajay Sharma [ID] * and Bikash Mohanty

For better utilization of 11 million tonnes of *Mangifera indica* wood (MIW) sawdust produced annually in India, the present study was planned for its characterization followed by determination of its pyrolysis kinetics from TGA data under a N_2 atmosphere. The characterization process included proximate-, ultimate-, biopolimeric components-, and heating value-analysis, as well as TG/DTG analysis. The distributed activation energy (DAE)- and Starink-methods were implemented on non-isothermal thermograms to compute the isoconversional values of activation energy for the pyrolysis of MIW. Further, the reaction mechanism for the pyrolysis of MIW was predicted using the Coats–Redfern (C–R) model-fitting method. Two distinct pyrolysis regions, region-I from 0.05−0.5 and region-II from 0.51−0.7, were observed in the complete conversion ranges. The estimated activation energy for region-I ranged from 143.03 to 176.46 kJ mol^{-1} with an average value of 157.12−157.97 kJ mol^{-1} and that of region-II varied between 143.03 and 161.68 kJ mol^{-1} with an average of 151.51−152.45 kJ mol^{-1}. The one-dimensional diffusion model (D_1) followed by the five and a half reaction order model ($F_{5.5}$) were recommended to describe the pyrolysis reaction mechanism of MIW for the two above regions, respectively. Further, the activation energies obtained *via* the DAE and Starink methods were used for the computation of thermodynamic parameters such as frequency factor, and change in-enthalpy, -entropy, and -Gibbs free energy.

1 Introduction

Due to an increase in population as well as industrial globalization, the energy sectors worldwide are facing challenges to fulfill the demand and supply gap of energy. Biomass – a carbon-neutral renewable resource, which can be derived from the carbonaceous waste of various human and natural activities, has become the third primary energy resource after coal and oil to bridge the above energy gap. Biomass can be derived from numerous sources, including the by-products from the timber industry, agro crops, raw material from the forest, major parts of household waste and wood. Therefore, the focus of research communities is now shifting from coal and oil to biomass which will not only produce energy which will be carbon neutral but also solve many problems including solid waste management, health hazards, wildfires, *etc.*

Parikka estimated the total worldwide energy potential from biomass, on a sustainable basis, to be 104 EJ per year, of which woody biomass, energy crops, and straw constituted 40.1%, 36%, and 16.6%, respectively.[1] Only about 40% of potential

biomass energy is currently utilized. The present global energy demand is about 470 EJ per year.[1] Forest residues, which remain largely unutilized, present solid waste disposal problems. Among these residues, wood sawdust, which is created as byproducts of the wood processing at wood cutting and furniture making industry, are generally generated in large quantity every year.[2] India is producing around 149 million cubic meters ($\approx$100 million tonnes) of *Mangifera indica* wood per year,[3] which when converted into planks will produce 11 million tonnes of sawdust. This sawdust is typically used in making of particle board and road laying. Still, a large amount of its waste is dumped around roadside, water bodies, and/or burn directly in an open environment, which creates anthropogenic hazard for all the living species and thus are an unacceptable solution. *Mangifera indica* wood is increasingly being used in furniture making, due to its pros as hardwood furniture material as well as its sustainability quotient. *Mangifera indica* species are found all around the world (major contributors are Bangladesh, Burma, Cambodia, China, Hawaii (US), India, Indonesia, Laos, Malaysia, Papua New Guinea, Philippines, Thailand, and Vietnam). *Mangifera indica* wood is readily available and is affordable compared to other timber species.

Reaction kinetics, which includes the computations of kinetic triplets (the activation energy, pre-exponential factor

Department of Chemical Engineering, Indian Institute of Technology, Roorkee, India, 247667. E-mail: asharma@ch.iitr.ac.in

and reaction models), is essentially required in order to understand the chemistry behind the thermal degradation of material and further to transform laboratory-scale studies to large-scale reactor conditions.[4] The procedures used for the computation of kinetic parameters (A, E, and n) of material degradation during solid–gas heterogeneous reactions include model-fitting and model-free methods, which have been extensively used in the thermal decomposition of solids, thermal degradation of polymers and crystallization of glasses.[5] TG-DTG coupled FTIR and/or GC-MS is widely used to extract information about material degradation and further to interpret the products released from the pyrolyzer unit.[6] The reaction kinetics provide deeper insights into the mechanism of solid thermal degradation which is important for the proper selection-, optimization- and operation – of a reactor.[7] Moreover, kinetic analysis of pyrolysis reaction further opens the path for the estimation of various thermodynamic parameters enthalpy (ΔH), Gibbs free energy (ΔG), and entropy (ΔS) of the pyrolysis process.[8] The thermodynamic parameters are essentially needed to design an efficient pyrolysis system and also for choosing the target biofuels.[9]

Amongst all thermochemical processes such as combustion, gasification, and pyrolysis, pyrolysis is the least energy-consuming process thus, the assessment of thermodynamic parameters on pyrolysis conditions is imperative. In all, kinetic parameters, reaction mechanism and thermodynamic parameters (change in-enthalpy, -Gibbs free energy, and -entropy) are important for the design, optimization, and scaling of process reactor.

Even though India is the largest producer of mango (*Mangifera indica*) wood in the world, scientific management of waste mango wood created during processing needs special attention. From literature review, it has been observed that there is hardly any research work conducted to study pyrolysis kinetics and its thermodynamic analysis for *Mangifera indica* wood (MIW). Also, a few research papers are available in an open literature that provides systematic kinetic and thermodynamic data of wood pyrolysis with detailed explanations of phenomena. Hence, the present study was planned to investigate the characterization of MIW sawdust, determination of pyrolysis kinetics and reaction mechanism. In addition, the thermodynamic parameters were computed to assess the feasibility of MIW pyrolysis for effective process designs and operations.

2 Materials and methods

2.1 Feedstock preparation

The MIW sawdust used as a raw material in this study was obtained from a sawmill at Meerut, Uttar Pradesh (India). The sawdust sample was then heated in an air oven at 35 °C for 24 hours and sieved to obtain an average particle size of 100 μm. The sieved sample (100 μm) was kept in a closed plastic zip-bag for the thermogravimetric analysis.

2.2 Chemical characterization of MIW

This section includes proximate-, ultimate-, heating value-, and biopolimeric components-analysis of MIW sample. The proximate analysis is the easiest and the fastest way of investigating the fuel potential of solid materials. It determines the moisture, volatile matter, ash, and fixed carbon content of the sample. The detailed evaluation of these on 1 g initial sample mass basis is given in Table 1.

Further, the elemental compositions (CHNS/O) of MIW sawdust were determined using an elemental analyzer (Perkin Elmer 2400, USA). The elemental compositions which include the determination of the mass% of carbon, hydrogen, nitrogen, sulfur, and oxygen content were then used for the computation of calorific value. The calorific value of material can be categorized as higher and lower heating values (HHV and LHV). The HHV and LHV measure the amount of energy which can be obtained from the unit quantity of material. The HHV and LHV were computed using the analytical expressions given by Channiwala and Parikh[10] and Basu,[11] respectively. In addition to it, mass% of extractives, hemicellulose, cellulose, and lignin were determined using Li et al.[12] The detailed experimental procedure is given elsewhere.[13]

2.3 Thermogravimetric/differential thermogravimetric (TG/DTG) analysis

In order to determine the thermal stability of material over the temperature range of 30 °C to 650 °C, the MIW sample was passed through a thermogravimetric (TG/DTG) analyzer (Seiko Model: SII 6300 EXSTAR, Japan). A non-isothermal TG/DTG analysis of the MIW sample was carried out at four different heating rates of 10, 20, 30, and 40 °C min^{-1}. For a given heating rate, 10 mg sample of MIW was taken in an alumina (Al$_2$O$_3$) crucible and was heated from ambient temperature to 650 °C. During the whole

Table 1 Procedure for the proximate analysis of *Mangifera indica* wood (MIW) with codes used^{a,b}

|	Moisture content (MC)	Volatile matter (VM)	Ash
Standard	ASTME871	ASTME872	ASTMD1102
Sample mass (initial)	1 g	m_1 g	m_2 g
Temperature	103 ± 2 °C	925 ± 5 °C	580–600 °C
Holding time	Until constant mass	7 min	4 h
Crucible	Silica spherical	Silica cylindrical	Silica cylindrical
Sample mass (final)	m_1 g	m_2 g	m_3 g
Calculation (%)	$(1 - m_1) \times 100$	$(m_1 - m_2) \times 100$	$m_3 \times 100$
Fixed carbon (mass%) = 100 − MC − VM − ash = $(m_2 - m_3) \times 100$			

^{a} Where m_1 = mass of the sample after moisture removal, m_2 = mass of sample after the removal of moisture and volatile matter, and m_3 = mass of ash content present in the sample. ^{b} All mass should be measured after cooling down the sample in a desiccator up to room temperature.

experiment, the flow of nitrogen gas (N_2(g); purity = 99.999%) was maintained at 100 ml min^{-1}, which created an inert environment around the sample. The TG-DTG data was further used for the computation of activation energy, frequency factor, change-of enthalpy, -entropy, and -Gibbs free energy. A detailed description of the methodology used for the determination of kinetics parameters is given in the next section.

2.4 Non-isothermal kinetic model for the pyrolysis reaction

To define the complete pyrolysis process is challenging as it involves enormous variations due to physical and chemical transformations while producing a large number of product species. As a result, thermal degradation of biomass is a heterogeneous reaction and as single-step global kinetics, it can be modeled as:

$$MIW(s) \xrightarrow{(N_2\text{-atmosphere})} a \text{ bio-char(s)} + b \text{ volatiles(tar + gases)}$$
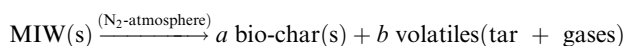
where a and b are the yield coefficients of the different products (bio-char and volatiles) of the pyrolysis. The rate expression for the above reaction:[14]

$$\frac{d\alpha}{dt} = k(T)f(\alpha) \tag{1}$$

where α stands for fractional conversion. T stands for absolute temperature. $\alpha = \left(\frac{m(T_i) - m(T)}{m(T_i) - m(T_f)}\right)$; $m(T_i)$ = initial sample mass, $m(T_f)$ = final sample mass, and $m(T)$ = instantaneous sample mass. The Arrhenius equation is useful for describing reaction rate constant '$k(T)$' of many thermally activated, heterogeneous solid-state reactions such as diffusion, nucleation and nuclei growth, presumably because the system has to overcome an energy barrier and energy distribution along the relevant coordinate is controlled by Boltzmann statistics. Therefore, $k(T) = A \exp(-E_a/RT)$; A = frequency factor, $\exp(-E_a/RT)$ = Boltzmann factor, E_a = apparent activation energy, R = universal gas constant. The factor $f(\alpha)$ represents the differential form of reaction model, which is a function of conversion and reaction order.

Therefore,

$$\frac{d\alpha}{dt} = A \exp\left(-\frac{E_a}{RT}\right)f(\alpha) \tag{2}$$

Further, a constant term β (=dT/dt) called heating rate is introduced as a conversion factor, used whenever required for the transformation of dynamic form into non-isothermal form. As in the present case, for non-isothermal TG kinetics, eqn (2) converts as below:

$$\frac{d\alpha}{dT} = \left(\frac{A}{\beta}\right)\exp\left(-\frac{E_a}{RT}\right)f(\alpha) \tag{3}$$

Integrating above on both sides:

$$\int_0^\alpha \frac{d\alpha}{f(\alpha)} = g(\alpha) = \int_{T_0}^{T_\alpha} \left(\frac{A}{\beta}\right)\exp\left(-\frac{E_a}{RT}\right)dT$$

or,

$$g(\alpha) = \int_0^{T_\alpha} \left(\frac{A}{\beta}\right)\exp\left(-\frac{E_a}{RT}\right)dT - \int_0^{T_0} \left(\frac{A}{\beta}\right)\exp\left(-\frac{E_a}{RT}\right)dT.$$

The second term in R.H.S is comparatively small. So, neglecting low-temperature end of the interval, the general form of all the integral isoconversional kinetic methods,

$$g(\alpha) \approx \int_0^{T_\alpha} \left(\frac{A}{\beta}\right)\exp\left(-\frac{E_a}{RT}\right)dT = \left(\frac{A}{\beta R}\right)\int_x^\infty E_a \frac{\exp(-x)}{x^2}dx,$$

$$\text{when } x = \frac{E_a}{RT_\alpha} \tag{4}$$

Here, $g(\alpha)$ is the integral form of the reaction model. TGA technique is used to determine the kinetic triplet [E, A, and reaction model $f(\alpha)$ or $g(\alpha)$]. If, for a given conversion (α), E_a value remains constant for the temperature integral ranging from 0 to T_α. Then, for non-isothermal TGA thermogram at constant heating rate, eqn (4) converts as below:

$$g(\alpha) = \frac{AE_\alpha}{\beta R}\int_x^\infty \frac{e^{-x}}{x^2}dx = \frac{AE_\alpha}{\beta R}p(x) \tag{5}$$

where $p(x)$ is termed as exponential/temperature integral. Here, $p(x) = p(E_a, T_\alpha)$. For a specific value of x, $p(x)$ has no analytical/exact solution. Therefore, various numerical approximations were reported and based on these approximations, different mathematical expressions were derived for the estimation of activation energy. In the present work, the activation energies were estimated using the distributed activation energy (DAE) and Starink methods. For a given conversion (α; $0 \le \alpha \le 1$), in Miura-Maki's DAE method:[15] $E_\alpha = R \times$ slope of $\ln\left(\frac{\beta_i}{T_{\alpha,i}{}^2}\right)$ vs. $\frac{1}{T_{\alpha,i}}$ whereas, in Starink method:[16] $E_\alpha = \left(\frac{R}{1.0008}\right) \times$ slope of $\ln\left(\frac{\beta_i}{T_{\alpha,i}{}^{1.8}}\right)$ vs. $\frac{1}{T_{\alpha,i}}$. Further, the E_α values obtained from these methods were used to predict the reaction mechanism. For this purpose, the Coats–Redfern (C–R) expression[17] was used. The details for the method is given below:

From eqn (4),

$$g(\alpha) \approx \int_0^{T_\alpha} \left(\frac{A}{\beta}\right)\exp\left(-\frac{E_a}{RT}\right)dT \cong$$

$$\frac{ART_\alpha{}^2}{\beta E_a}\left(1 - \frac{2RT_\alpha}{E_a}\right)\exp E_a/RT_\alpha; \tag{6}$$

if the term $(1/T)$ having order higher than two are ignored.

Assuming $(1 - 2RT/E_a) \approx 1$ and taking $\log_e$ of eqn (6), the final expression becomes:

$$\ln[g(\alpha)/T_\alpha{}^2] = -(E_a/RT_\alpha) + \ln(AR/\beta E_a) \tag{7}$$

Based on mechanistic assumptions, reaction models are divided into nucleation, geometrical contraction, diffusion, and reaction order.[18] Under nucleation models, the formation and growth of nuclei are considered to be rate-limiting. In geometrical contraction, the progress of product layer from the surface

to the inner boundary is considered to be rate-limiting. In diffusion, the diffusion of reactant or product is considered to be rate-limiting. And finally, in reaction order based model, the rate law is based on homogeneous kinetics. Based on the above mechanisms, the integral form of the reaction model [$g(\alpha)$] was decided. Table 2 lists different models as a function of the extent of conversion. Here, $g(\alpha)$ is approximated to defined linear or non-linear expressions based on conversion (α) and order of reaction (n). Corresponding to each kinetic mechanism, a global value of activation energy (E_a) and pre-exponential factor (A) was obtained.

2.5 Thermodynamic parameters calculation

With the obtained activation energy from isoconversional methods, the value of T_m from DTG curve and T_α from TGA thermogram, the thermodynamic parameters including the frequency factor (A), change-of enthalpy (ΔH), -entropy (ΔS), and -Gibbs free energy (ΔG) are all functions of heating rates, and can be computed by the following equations:[8]

$$A_\alpha = \beta E_\alpha \, \exp\left(\frac{E_\alpha}{RT_m}\right) \bigg/ \left(RT_m^2\right) \quad (8)$$

$$\Delta H_\alpha = E_\alpha - RT_\alpha \quad (9)$$

$$\Delta G_\alpha = E_\alpha + RT_m \, \ln\left(\frac{K_B T_m}{hA_\alpha}\right) \quad (10)$$

$$\Delta S_\alpha = \frac{\Delta H_\alpha - \Delta G_\alpha}{T_m} \quad (11)$$

where, K_B represents Boltzmann constant (1.38×10^{-23} J K^{-1}), h Planck's constant (6.67×10^{-34} J s), T_m the DTG peak temperature (K), T_α is the temperature (K) at the degree of conversion (α), and R is the universal gas constant (0.008314 kJ mol^{-1} K^{-1}).

Moreover, the energy barriers (EB) for the formulation of activated complex from the initial reactants were also computed.

Mathematically,

$$\text{EB} = E_\alpha - \Delta H_\alpha. \quad (12)$$

3 Results and discussion

3.1 Characterization of MIW

Table 3 exhibits the results of the chemical characterization of MIW.

The proximate analysis of MIW shows volatiles and fixed carbon as 73.38 mass% and 15.09 mass% with moisture and ash content as 7.06 mass% and 4.47 mass%, respectively. The adequate amount of volatiles (73.38 mass%) in MIW facilitates the thermal conversion process, as they lead to more combustible gases during the conversion, which further converts to bio-oil by the condensation process. The fixed carbon in MIW (15.09 mass%) is also an important element as it gets converted into biochar during the pyrolysis.[21] Further, the moisture content of 7.06 mass%, in MIW can be considered as low,[22] meaning that it can be removed with a small amount of additional energy. The low ash content in MIW (4.47 mass%) indicates its fast thermal degradation since with high ash content biomass will tend to form slag and may cause fouling problems in many thermal conversion

Table 2 Algebraic expressions for $g(\alpha)$ for the most frequently used mechanisms of solid-state thermal degradation[19,20]

Degradation mechanisms		Differential form: $f(\alpha)$	Integral form $= g(\alpha) \int_0^\alpha \frac{d\alpha}{f(\alpha)}$
Nucleation models			
A$_2$	Avrami–Erofe'ev	$2(1-\alpha)[-\ln(1-\alpha)]^{1/2}$	$[-\ln(1-\alpha)]^{1/2}$
A$_3$	Avrami–Erofe'ev	$3(1-\alpha)[-\ln(1-\alpha)]^{2/3}$	$[-\ln(1-\alpha)]^{1/3}$
A$_4$	Avrami–Erofe'ev	$4(1-\alpha)[-\ln(1-\alpha)]^{3/4}$	$[-\ln(1-\alpha)]^{1/4}$
Reaction-order models			
F$_0$/R$_1$	Zero-order	1	α
F$_1$	First-order	$(1-\alpha)$	$-\ln(1-\alpha)$
F$_2$	Second-order	$(1-\alpha)^2$	$[1-(1-\alpha)^{-1}]/-1$
F$_3$	Third-order	$(1-\alpha)^3$	$[1-(1-\alpha)^{-2}]/-2$
F$_4$	Fourth-order	$(1-\alpha)^4$	$[1-(1-\alpha)^{-3}]/-3$
F$_5$	Fifth-order	$(1-\alpha)^5$	$[1-(1-\alpha)^{-4}]/-4$
F$_{5\frac{1}{2}}$	Five and a half-order	$(1-\alpha)^{5.5}$	$[1-(1-\alpha)^{-4.5}]/-4.5$
Diffusion models			
D$_1$	One dimensional	$(1/2)\alpha$	α^2
D$_2$	Two dimensional (Valensi)	$[-\ln(1-\alpha)]^{-1}$	$(1-\alpha)\ln(1-\alpha)+\alpha$
D$_3$	Three dimensional (Jander)	$3(1-\alpha)^{2/3}/2(1-(1-\alpha)^{1/3})$	$[1-(1-\alpha)^{1/3}]^2$
D$_4$	Three dimensional (Ginstling–Brounshtein)	$(3/2)[(1-\alpha)^{-1/3}-1]$	$[1-(2/3)\alpha]-(1-\alpha)^{2/3}$
Geometrical contraction models			
R$_2$	Contracting area	$2(1-\alpha)^{1/2}$	$1-(1-\alpha)^{1/2}$
R$_3$	Contracting volume	$3(1-\alpha)^{2/3}$	$1-(1-\alpha)^{1/3}$

Table 3 Results of proximate-, ultimate- and biopolimeric components -analysis of MIW

	MIW
Proximate analysis (mass%)	
Moisture content	7.06
Volatile matter	73.38
Ash	4.47
Fixed carbon	15.09
Ultimate analysis (mass%)	
C	38.98
H	5.065
N	0.08
S	0.00
O[a]	44.345
HHV (MJ kg^{-1})	14.89
LHV (MJ kg^{-1})	13.64
H/C molar ratio	1.559
O/C molar ratio	0.853
Empirical formula[b]	$CH_{1.559}O_{0.853}N_{0.002}$
Biopolimeric components (mass%)	
Extractives	5
Hemicellulose	25
Cellulose	46.25
Lignin	23.75

[a] O_2 content (mass%) $= 100 - C$ (mass%) $- H$ (mass%) $- N$ (mass%) $- S$ (mass%) $-$ ash (mass%) $-$ moisture (mass%). [b] Empirical formula of MIW was developed using its ultimate analysis data.

conveying parts. The moisture and ash content found in proximate analysis refers to the same moisture and ash as reported in the ultimate analysis. However, in the proximate analysis, obtained fixed carbon as 15.09 mass% differs from the reported carbon in the ultimate analysis which is 38.98 mass%. The plausible reason for this difference is that %C measured in ultimate analysis is the total mass% of carbon in MIW, including the carbon in volatile matter. Also, the sulfur content in MIW is 0 mass%. This indicates its favorability as there are no concerns related to SO_2 emission & equipment corrosion when using it as a fuel. The HHV and LHV of

MIW were computed as 14.89 MJ kg^{-1} and 13.64 MJ kg^{-1}, respectively. The empirical formula of MIW was obtained as $CH_{1.559}O_{0.853}N_{0.002}$. Moreover, the biopolimeric components of MIW such as extractives, hemicellulose, cellulose and lignin (in mass%) were found as 5, 25, 46.25 and 23.75, respectively.

3.2 Interpretation of TG-DTG plots for MIW pyrolysis

The mass loss curves (TG) and rate of mass loss curves (DTG) for MIW sample in nitrogen atmosphere over a period of temperature, at four heating rates of 10, 20, 30, and 40 °C min^{-1}, are presented in part a and *b* of Fig. 1, respectively. The thermal decomposition profiles show that the entire pyrolysis of MIW can be divided into three zones (Fig. 1a).

Zone I. Removal of weakly bonded H_2O molecules and hydrolysis of some extractive components present in MIW were observed at temperature up to 200 °C with a minor mass loss of ~8 mass%. This zone is called dehydration.

Zone II. This is the major zone (200 to 400 °C) of pyrolysis process in which biomass is completely dried and majority of volatiles are released in this zone (Fig. 1a). Here, the thermal cracking of three compounds (25 mass% hemicellulose, 46.25 mass% cellulose, and 23.75 mass% lignin in MIW) is dominant and the thermal reactivity goes on increasing as the reaction temperature increases. For the pyrolysis of MIW, the highest reactivity (in terms of mass loss percent) amongst hemicellulose, cellulose, and lignin components was observed (41.12%) for 10 °C min^{-1} and lowest (34.57%) was for 40 °C min^{-1}. This indicates that the rate of volatilization is a function of heating rates. During the degradation process from 200 to 400 °C, a range of volatiles components (condensable and non-condensable) are released. In this range, the condensable fraction is the precursors of the liquid bio-oil. Zone II of Fig. 1b (200 °C to 400 °C) is characterized by the formation of one shoulder and a well-defined peak at ~300 °C and 325 °C, ~310 °C and 335 °C, ~320 °C and 338 °C, and ~330 °C and 343 °C, for 10 °C min^{-1}, 20 °C min^{-1}, 30 °C min^{-1}, and 40 °C min^{-1}, respectively. As per previous research on wood composites,[23,24] hemicellulose reacts between 230 °C to 330 °C
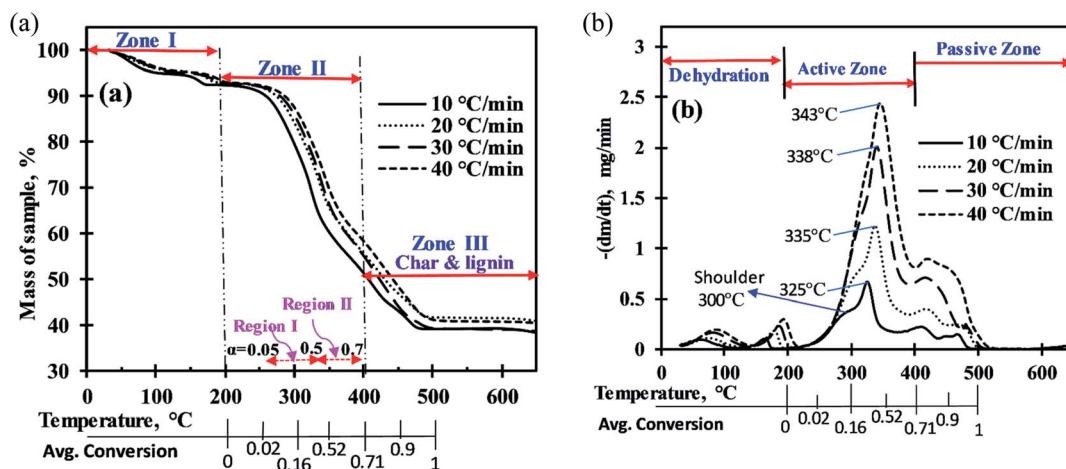

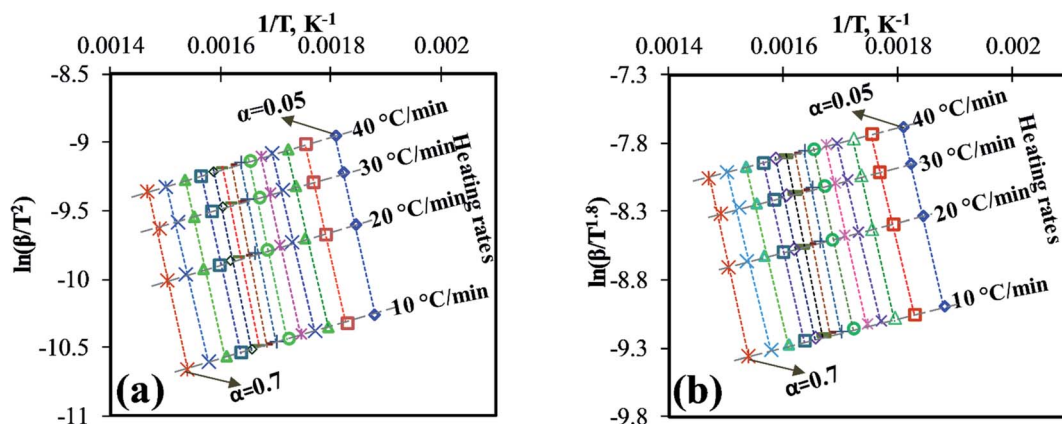**Fig. 1** (a) Mass loss (%) of MIW with rise in temperature, (b) mass loss rate (mg min^{-1}) of MIW with rise in temperature.

Fig. 2 (a) DAE plot for E_α, (b) Starink plot for E_α.

corresponds to the shoulders in DTG curves (Fig. 1b). The cellulose degrades between 270 °C to 370 °C corresponds to the main peak, and the lignin degrades over a wide temperature range from 200 °C to 650 °C corresponds to the remaining peaks.

Zone III. This zone (from 400 °C to 650 °C) belongs to the massive thermal decomposition of lignin and is called passive pyrolysis zone,[25] as shown in TG-DTG curves. The mass loss% in this zone was 16.2%, 16.8%, 17.9%, and 19.16% for 10, 20, 30, and 40 °C min^{-1}, respectively. The residue obtained here is solid biochar which further oxidized to form CO_2, CO, and $H_2O(g)$.

3.3 Kinetic analysis

For the computation of kinetic parameters during the pyrolysis of MIW in the temperature range of 200 °C to 500 °C, the associated range of conversion was divided into a number of differential sub-zones having conversion difference ($\Delta\alpha$) equal to 0.05 and for each sub-zone kinetic parameters were computed based on TG-DTG thermograms. The activation energies were determined by DAE and Starink methods using non-isothermal TG-DTG thermograms at four different heating rates (10, 20, 30, and 40 °C min^{-1}).

Fig. 2a and b depict the regression line plots of DAE and Starink methods, respectively. Fig. 2a and b shows that for conversions between 0.05 and 0.7, the correlation coefficients

(R^2) for above linear fit methods are close to unity. In the present study, depending upon the heating rates [$\beta_{(1-4)} = 10, 20, 30,$ and 40 °C min^{-1}], the kinetic parameters were computed in the conversion range 0.05 to 0.7 which corresponds to a temperature range of 200 °C to 395 ± 15 °C. After a fractional conversion of 0.7, the computed activation energies (E_α) were not taken into consideration as these were unreliable due to low value of correlation coefficient (R^2). The average activation energy (in kJ mol^{-1}) computed using DAE and Starink methods were found to be 154.86 and 155.74, respectively. Table 4 enlists the comparison of average activation energy of MIW with other biomass reported in the literature using isoconversional methods. The matching of average E-values of MIW with other biomass such as poplar wood,[26] eucalyptus wood,[27] European beech wood,[28] and sal wood[29] makes it suitable for the co-pyrolysis with several other biomass feedstocks.

In reference to Fig. 3, For $0.05 \leq \alpha \leq 0.1$ (avg. temperature from 270 to 288 °C), the decrease in activation energy was noticed which indicates first breaking of the strong hemicellulose–lignin linkage then the comparatively weaker hemicellulose–cellulose and lignin–cellulose linkage.[36,37] Then, the activation energy remains almost constant for $0.1 < \alpha \leq 0.2$ (289 to 306 °C), indicating no severe bond cracking in this conversion range (Fig. 1b). After that, for $0.2 < \alpha \leq 0.4$ (307 to 334 °C), an increase in activation energies attributes to the thermal

Table 4 Comparison of average activation energy of MIW with other biomass reported in the literature using isoconversional methods

| Biomass feedstock	Heating rates (°C min^{-1})	Average activation energy (kJ mol^{-1})	References
MIW	10, 20, 30, 40	154.86–155.74	Present work
Dalbergia sissoo wood	5, 10, 15, 20, 30	136.06–147.75	30
Pine wood	5, 10, 20, 40	181.00–181.28	31
Babool wood	10, 15, 20	91.6 ± 4.7 to 102.7 ± 6.06	32
Wood sawdust	5, 10, 20	164.24–173.41	33
Poplar wood	2, 5, 10, 15	157.27–158.58	26
Eucalyptus wood	10, 40	108.39–192.93	27
European beech wood	5, 10, 15, 25, 35, 50	157.20–185.40	28
Pine sawdust	5, 10, 15, 20, 25	168.58–206.62	29
Sal wood		148.44–181.53	
Areca nut husk		160.45–184.61	
Olive wood	5, 10, 20, 40, 100	54.05–116.78	34
Invasive Reed Canary	10, 20, 30, 40	159.61–161.29	35
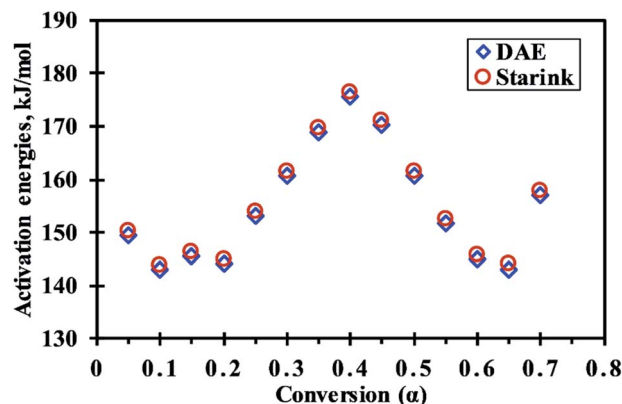
Fig. 3 Variation of activation energies (E_α) with conversion (α) during progress of reaction.

cracking of strong bonds (aromatic rings, C=O, C(=O)OH, C–C bonds within and between the alkyl chains) inside the biopolimeric components.[38] Further, for $0.4 < \alpha \leq 0.65$ (335 to 379 °C), the decrement in activation energies might be due to the breaking of C–OH and aliphatic groups, which requires comparatively less energy to break.[39] After that, for $0.65 < \alpha \leq 0.7$ (380 to 395 °C), the increment in activation energy indicates requirement of additional energy to benzene ring, aliphatic

groups, methyl groups, and methoxy groups at *ortho* position of hydroxyl group in MIW.[38] In the present study, the pattern of change in activation energies with conversion values is more consistent with the other biowastes such as *Prosopis juliflora*,[40] pine, sal and areca nut sawdust.[29] The change in activation energy with respect to conversion (Fig. 3) was due to the complex nature of pyrolysis reaction which shows the involvement of parallel, complex and competitive reactions.[41]

3.4 Prediction of degradation mechanism for the pyrolysis reaction of MIW

The C–R method was applied on thermogravimetric analysis (TGA) data at four different heating rates (10, 20, 30, and 40 °C min^{-1}) to obtained E-values based on various solid-state thermal degradation mechanisms (Table 5).

For better linear trend fitting ($R^2 > 0.97$) of data between ln $[g(\alpha)/T_\alpha^2]$ against $1/T_\alpha$ for all four heating rates, the conversion (α) range can be divided into two regions (Fig. 1a), region-I ($0.05 \leq a \leq 0.5$) and region-II ($0.51 \leq \alpha \leq 0.7$). These ranges were based on primary analysis.

Depending on the degradation mechanism, the functional relationship of the function $g(\alpha)$ changes as can be seen from Table 5. As per C–R method, plots between $\ln[g(\alpha)/T_\alpha^2]$ against

Table 5 Activation energy values for different solid-state thermal degradation mechanisms based on Coats–Redfern method[17]

Region	Reaction model	$g(\alpha)$	10 °C min^{-1} E, kJ mol^{-1}	R^2	20 °C min^{-1} E, kJ mol^{-1}	R^2	30 °C min^{-1} E, kJ mol^{-1}	R^2	40 °C min^{-1} E, kJ mol^{-1}	R^2	Average E-values E, kJ mol^{-1}	R^2
I	A_2	$[-\ln(1-\alpha)]^{1/2}$	37.35	0.99	37.46	0.99	40.15	0.99	39.28	0.99	38.56	0.99
	A_3	$[-\ln(1-\alpha)]^{1/3}$	21.76	0.98	21.76	0.99	23.52	0.99	22.91	0.99	22.49	0.99
	A_4	$[-\ln(1-\alpha)]^{1/4}$	13.96	0.98	13.91	0.99	15.20	0.99	14.72	0.99	14.45	0.98
	F_0	α	73.09	0.98	73.49	0.98	78.30	0.98	76.83	0.99	75.43	0.98
	F_1	$-\ln(1-\alpha)$	84.15	0.99	84.56	0.99	90.04	0.99	88.38	0.99	86.78	0.99
	F_2	$[1-1/(1-\alpha)]/-1$	96.56	1.00	96.96	1.00	103.19	1.00	101.32	1.00	99.51	1.00
	F_3	$[1-1/(1-\alpha)^2]/-2$	110.27	1.00	110.67	1.00	117.72	1.00	115.62	1.00	113.57	1.00
	F_4	$[1-1/(1-\alpha)^3]/-3$	125.22	1.00	125.61	1.00	133.56	1.00	131.22	1.00	128.90	1.00
	F_5	$[1-1/(1-\alpha)^4]/-4$	141.30	0.99	141.68	0.99	150.60	0.99	148.00	0.99	145.39	0.99
	$F_{5.5}$	$[1-1/(1-\alpha)^{4.5}]/-4.5$	149.73	0.99	150.10	0.99	159.53	0.99	156.79	0.99	154.04	0.99
	D_1	α^2	155.61	0.98	156.62	0.99	166.35	0.99	163.49	0.99	160.52	0.99
	D_2	$(1-\alpha)\ln(1-\alpha) + \alpha$	162.56	0.99	163.57	0.99	173.71	0.99	170.74	0.99	167.65	0.99
	D_3	$[1-(1-\alpha)^{1/3}]^2$	170.08	0.99	171.09	0.99	181.68	0.99	178.58	0.99	175.36	0.99
	D_4	$[1-(2/3)\alpha]-(1-\alpha)^{2/3}$	165.07	0.99	166.07	0.99	176.36	0.99	173.36	0.99	170.21	0.99
	R_2	$1-(1-\alpha)^{1/2}$	78.45	0.99	78.86	0.99	84.00	0.99	82.43	0.99	80.94	0.99
	R_3	$1-(1-\alpha)^{1/3}$	80.32	0.99	80.72	0.99	85.97	0.99	84.38	0.99	82.85	0.99
II	A_2	$[-\ln(1-\alpha)]^{1/2}$	8.76	0.91	8.98	0.96	8.90	0.97	8.00	0.95	8.66	0.95
	A_3	$[-\ln(1-\alpha)]^{1/3}$	2.37	0.61	2.43	0.79	2.35	0.84	1.70	0.67	2.21	0.73
	A_4	$[-\ln(1-\alpha)]^{1/4}$	—	—	—	—	—	—	—	—	—	—
	F_0	α	12.82	0.89	13.20	0.94	13.15	0.96	12.07	0.94	12.81	0.93
	F_1	$-\ln(1-\alpha)$	27.93	0.96	28.61	0.98	28.56	0.99	26.89	0.98	28.00	0.98
	F_2	$[1-1/(1-\alpha)]/-1$	48.64	0.98	49.70	0.99	49.64	1.00	47.18	0.99	48.79	0.99
	F_3	$[1-1/(1-\alpha)^2]/-2$	74.47	0.99	75.99	1.00	75.91	1.00	72.46	1.00	74.71	1.00
	F_4	$[1-1/(1-\alpha)^3]/-3$	104.22	0.99	106.27	1.00	106.19	1.00	101.59	1.00	104.57	1.00
	F_5	$[1-1/(1-\alpha)^4]/-4$	136.62	0.99	139.24	1.00	139.14	1.00	133.31	1.00	137.08	1.00
	$F_{5.5}$	$[1-1/(1-\alpha)^{4.5}]/-4.5$	153.46	1.00	156.39	1.00	156.28	1.00	149.80	1.00	153.98	1.00
	D_1	α^2	36.07	0.94	37.07	0.97	43.18	0.95	35.02	0.97	37.83	0.96
	D_2	$(1-\alpha)\ln(1-\alpha) + \alpha$	44.41	0.96	45.58	0.98	52.11	0.96	43.22	0.98	46.33	0.97
	D_3	$[1-(1-\alpha)^{1/3}]^2$	54.97	0.97	56.35	0.99	63.24	0.97	53.58	0.99	57.04	0.98
	D_4	$[1-(2/3)\alpha]-(1-\alpha)^{2/3}$	47.90	0.96	49.14	0.98	55.79	0.97	46.64	0.98	49.87	0.97
	R_2	$1-(1-\alpha)^{1/2}$	19.69	0.94	20.21	0.97	23.54	0.95	18.80	0.97	20.56	0.96
	R_3	$1-(1-\alpha)^{1/3}$	22.28	0.95	22.85	0.98	26.27	0.96	21.34	0.98	23.19	0.97

$1/T_\alpha$ were created for various degradation mechanisms to determine the value of E (slope of the linear trend line in Fig. 4a and b) for each of these degradation mechanisms at different heating rates as reported in Table 5. Then the E-values of a given degradation mechanism for all the four heating rates were added to produce an average E-value to be compared with average E-values determined using DAE and Starink methods. As per C–R method, if for a given degradation mechanism, these
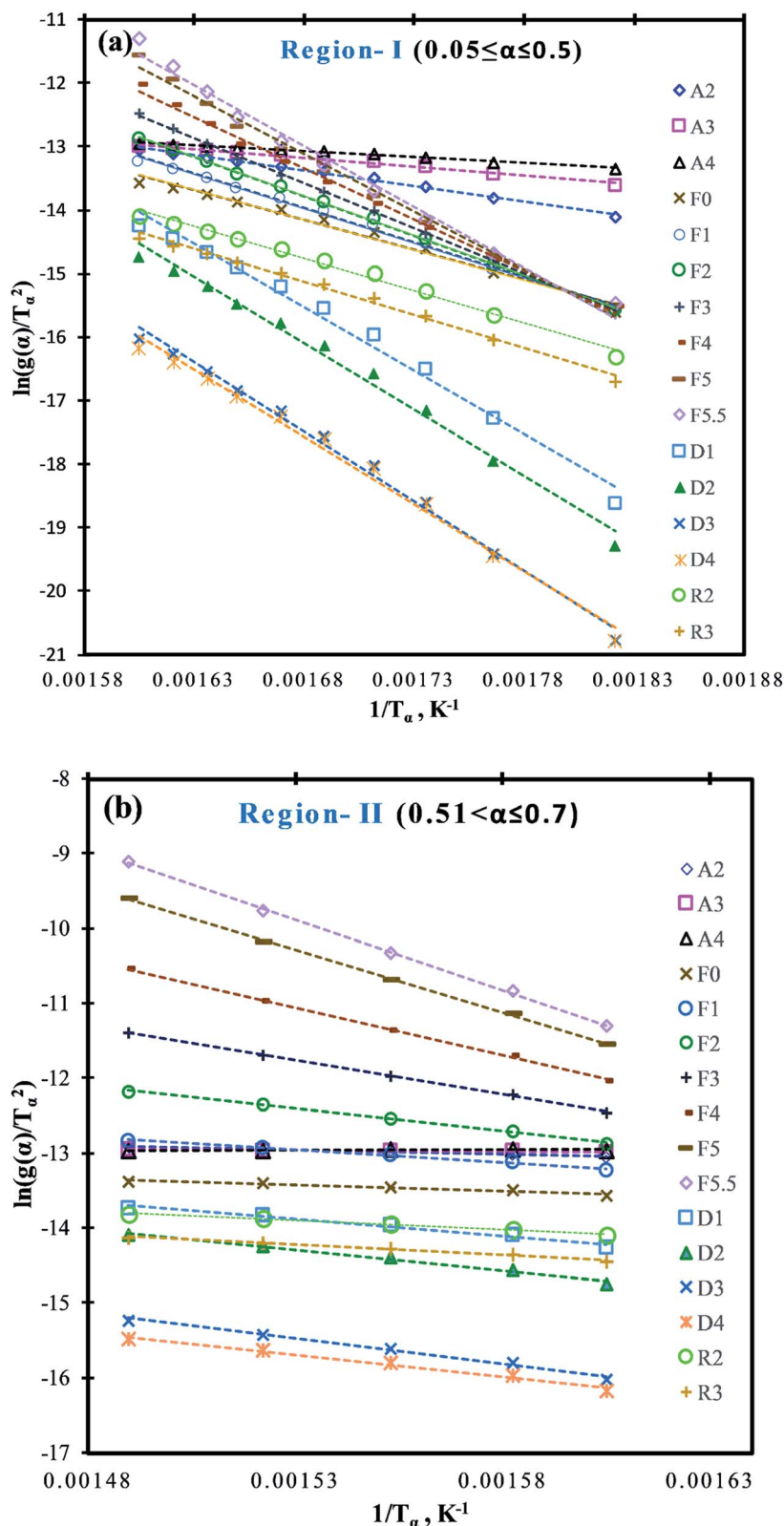

Fig. 4 C–R plots for the pyrolysis of MIW; (a) region-I ($0.05 \leq \alpha \leq 0.5$) and (b) region-II ($0.51 \leq \alpha \leq 0.7$).

Table 6 Activation energy and thermodynamic parameters during the pyrolysis process of MIW under the heating rate of 30 °C min⁻¹

	DAE method							Starink method						
α	E_α, kJ mol⁻¹	A_α, min⁻¹	k, min⁻¹	ΔH_α, kJ mol⁻¹	ΔG_α, kJ mol⁻¹	ΔS_α, J mol⁻¹ K⁻¹	Energy barrier, kJ mol⁻¹	E_α, kJ mol⁻¹	A_α, min⁻¹	k, min⁻¹	ΔH_α, kJ mol⁻¹	ΔG_α, kJ mol⁻¹	ΔS_α, J mol⁻¹ K⁻¹	Energy barrier, kJ mol⁻¹
0.05	149.54	8.8×10^{12}	0.05	144.98	151.43	−10.57	4.56	150.33	1.0×10^{13}	0.05	145.77	151.40	−9.23	4.56
0.1	143.03	2.3×10^{12}	0.15	138.32	151.66	−21.83	4.71	143.84	2.8×10^{12}	0.15	139.13	151.63	−20.45	4.71
0.15	145.43	3.8×10^{12}	0.25	140.64	151.57	−17.90	4.79	146.25	4.5×10^{12}	0.25	141.46	151.54	−16.51	4.79
0.2	144.20	3.0×10^{12}	0.38	139.34	151.62	−20.09	4.86	145.04	3.5×10^{12}	0.38	140.18	151.59	−18.66	4.86
0.25	153.03	1.8×10^{13}	0.56	148.11	151.31	−5.25	4.92	153.88	2.1×10^{13}	0.56	148.96	151.29	−3.81	4.92
0.3	160.68	8.5×10^{13}	0.83	155.70	151.07	7.58	4.98	161.53	1.0×10^{14}	0.83	156.55	151.04	9.02	4.98
0.35	168.79	4.4×10^{14}	1.26	163.75	150.82	21.17	5.04	169.65	5.2×10^{14}	1.27	164.61	150.79	22.62	5.04
0.4	175.59	1.7×10^{15}	1.72	170.51	150.62	32.56	5.08	176.46	2.1×10^{15}	1.73	171.38	150.59	34.02	5.08
0.45	170.17	5.8×10^{14}	2.28	165.04	150.77	23.35	5.13	171.05	7.0×10^{14}	2.30	165.92	150.75	24.83	5.13
0.5	160.78	8.7×10^{13}	2.88	155.60	151.06	7.42	5.18	161.68	1.0×10^{14}	2.91	156.50	151.03	8.94	5.18
0.55	151.72	1.4×10^{13}	3.96	146.47	151.36	−8.01	5.25	152.64	1.7×10^{13}	4.01	147.39	151.33	−6.45	5.25
0.6	144.99	3.5×10^{12}	6.05	139.64	151.59	−19.56	5.35	145.93	4.2×10^{12}	6.15	140.58	151.56	−17.97	5.35
0.65	143.03	2.3×10^{12}	9.95	137.57	151.66	−23.06	5.46	144.00	2.8×10^{12}	10.15	138.54	151.63	−21.42	5.46
0.7	157.04	4.0×10^{13}	24.32	151.46	151.18	0.45	5.58	158.02	4.9×10^{13}	24.90	152.44	151.15	2.11	5.58

two average values match well, then the given degradation mechanism is considered to be the prevailing one.

It is shown from Table 5 that in region-I, the average E-values are different for different reaction mechanisms characterized by different functional relationship of $g(\alpha)$, under all the four different heating rates. For random nucleation (A_2, A_3, and A_4) and contraction geometry (R_2 and R_3) mechanisms, the average E-values ranged from 14.45 to 38.56 kJ mol⁻¹ and 80.94 to 82.85 kJ mol⁻¹ respectively. Further, for the reaction order model (F_0, F_1, F_2, F_3, F_4, F_5, and $F_{5.5}$), the average E-values of four heating rates ranged from 75.43 to 154.04 kJ mol⁻¹, whereas in the diffusion model (D_1, D_2, D_3, and D_4) these values ranged from 160.52 to 175.36 kJ mol⁻¹ which were closest to the average E-values obtained from DAE (157.12 kJ mol⁻¹) and Starink (157.97 kJ mol⁻¹) methods. Thus it can be safely concluded that diffusion appears to be the rate-determining step for the pyrolysis reaction of MIW at the initial stage ($0.05 \leq \alpha \leq 0.5$), denoted by region-I.

Diffusion based models assume that the reaction rate is higher than reaction front propagation throughout the pyrolysis medium. Accordingly, the pyrolytic degradation reaction occurs at the boundary of the two phases like solid and gas. Therefore, the gas must diffuse into the formed product layer around the sample to reach to the unreacted solid for a reaction to progress and thus makes diffusion the rate-determining step.

Similarly, for region-II ($0.51 \leq \alpha \leq 0.7$) the average E-values for different reaction order models ranged from 12.81 for zeroth order (F_0) to 153.98 kJ mol⁻¹ for five and a half order reaction ($F_{5.5}$) model. However, it can be seen that the E-values obtained from DAE ($=151.51$ kJ mol⁻¹) and Starink methods ($=152.45$ kJ mol⁻¹) were close to the five and half order reaction model indicating that region-II is a five and a half order reaction controlled region.

Therefore, the mechanism for the pyrolysis reaction of MIW was one-dimensional diffusion model (D_1; region-I: $0.05 \leq \alpha \leq 0.5$) followed by five and a half order ($F_{5.5}$; region-II: $0.51 \leq \alpha \leq 0.7$) reaction, which is proportional to the concentration of reactant(s) in a particular reaction. The reaction mechanism obtained in present work for pyrolysis of MIW is consistent with the earlier research[30,42,43] (i.e. for *Dalbergia sissoo* wood[30] it was governed by D_3 followed by F_3 controlled, for waste tea[42] D_3 followed by F_2, and for four different wood species[43] $D_{1,2,3}$ followed by F_1).

3.5 Estimation of thermodynamic parameters

In order to check the feasibility of the pyrolysis reaction, the thermodynamic parameters are essentially needed. The frequency factor, change-in enthalpy, -Gibbs free energy, and -entropy corresponding to the value of α were computed using eqn (8)–(11), respectively for DAE and Starink methods, and the obtained results from the analysis are presented in Table 6 and have been illustrated in Fig. 5a, b, d and e, respectively.

The frequency factor (A_α) for each value of a were computed using eqn (8) and found to vary from 2.3×10^{12} min⁻¹ to 1.7×10^{15} min⁻¹ for DAE and 2.8×10^{12} min⁻¹ to 2.1×10^{15} min⁻¹ for Starink methods for α value varying from 0.1 (around 293 °C)
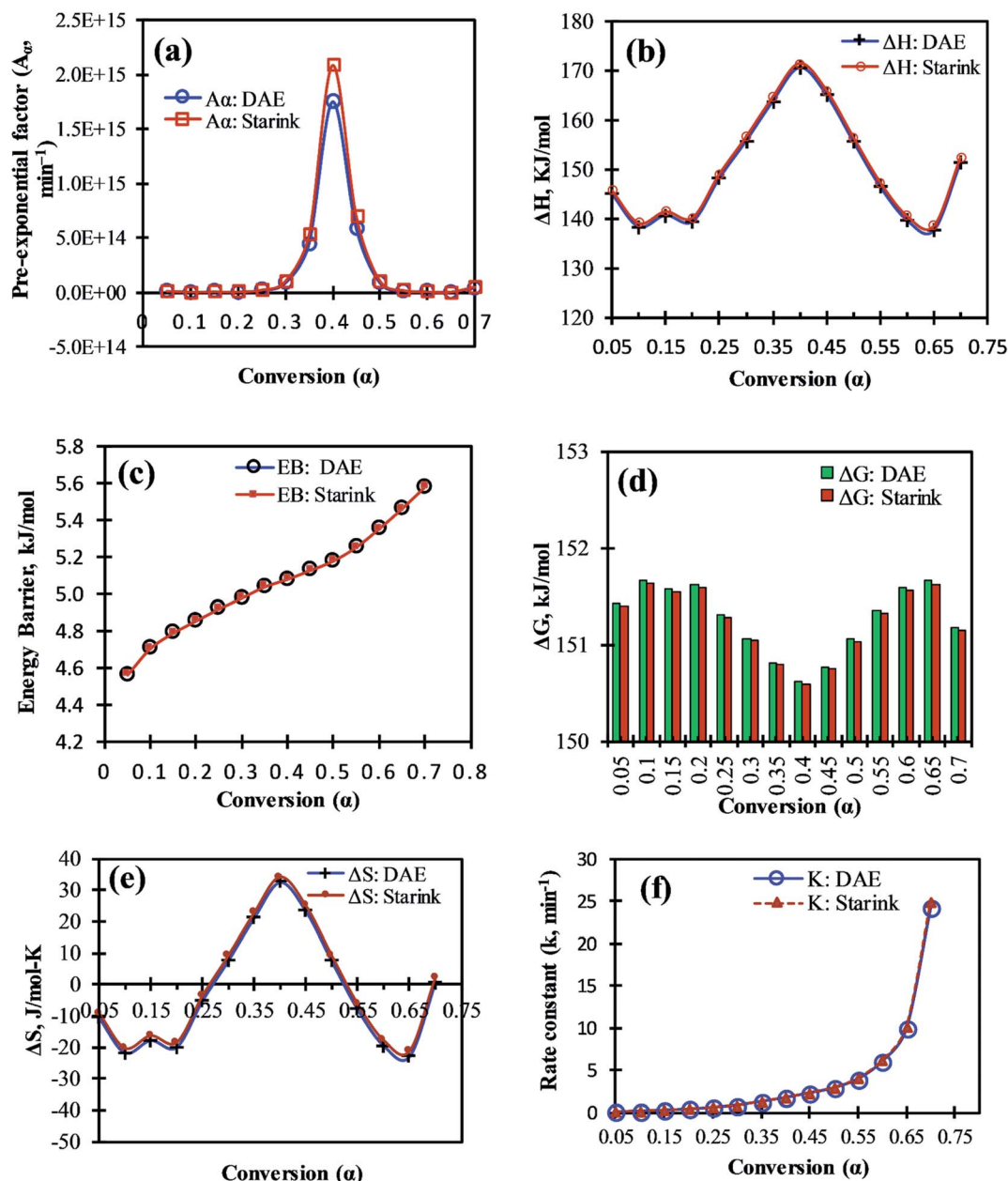
Fig. 5 (a) Pre-exponential factor with conversion during MIW pyrolysis, (b) change in enthalpy with conversion during MIW pyrolysis, (c) energy barrier over the range of conversion, (d) change in Gibbs free energy with conversion, (e) change in entropy with conversion, (f) reaction rate constant with conversion.

to 0.4 (around 338 °C). It is a fact that if $A_\alpha < 10^9$ min^{-1}, it is considered as low and often indicates less surface reactivity of the system.[44] In present case, higher A_α values were noticed for $0.3 \leq \alpha \leq 0.5$ (from 8.5×10^{13} min^{-1} to 2.1×10^{15} min^{-1}), which corresponds to the temperature range of 326–350 °C, indicating high surface reactivity of MIW particle along with formation of a simple activated complex.[45] From Fig. 5a and Table 6, the value of A_α was relatively lower at hemicellulose shoulder (at $\alpha = 0.25$, $T = 320$ °C, $A_\alpha = 1.8 \times 10^{13}$ or 2.1×10^{13} min^{-1}) than the main peak of cellulose (at $\alpha = 0.4$, $T = 338$ °C, $A_\alpha = 1.7 \times 10^{15}$ or 2.1×10^{15} min^{-1}) for the pyrolysis of MIW, indicating a comparative lower rate of molecular collisions for the hemicellulose component.

Fig. 5b shows that all values of ΔH_α are positive. This indicates the endothermic nature of the pyrolysis reaction. The highest and lowest values of ΔH_α recorded were 171.38 kJ mol^{-1} at $\alpha = 0.4$ (338 °C) and 137.57 kJ mol^{-1} at $\alpha = 0.65$ (384 °C), respectively. The highest and lowest positive value of ΔH_α attributes to the maximum and minimum dissociation of MIW during its pyrolysis at 338 °C and 384 °C, respectively and it is also evident from DTG thermogram of MIW (Fig. 1b). The ΔH_α value increased for α from 0.2 to 0.4 and 0.65 to 0.7 indicating an increase in endothermicity of MIW pyrolysis in these ranges. However, for other ranges of α such as 0.05 to 0.1 and 0.4 to 0.65, it gradually decreased indicating a comparative decrease in endothermicity of reaction in these ranges. For α ranging

from 0.05 to 0.7, the average ΔH values determined by DAE and Starink methods were 149.79 and 150.67 kJ mol^{-1}. For the present case, values of ΔH_α and activation energy (E_α) values followed the same trend. This trend is similar to the trends observed for pyrolysis process of lignocellulosic biomass, such as castor residue[46] and garlic stalk.[47] The difference between ΔH_α and E_α corresponds to the energy barriers (EB) for the formation of activated complex for the reactants.[48] A reaction having a higher energy barrier requires a higher temperature to be conducted. In the present case, the energy barrier for reaction increases (from 4.56 to 5.58 kJ mol^{-1}) as evident from Fig. 5c when conversion increases from 0.05 to 0.7. During this, the temperature also increases from 276 to 398 °C and thus helps to overcome the energy barrier of required for the reactions to take place. The small value of EB (≈ 5.06 kJ mol^{-1}) during complete reaction period indicates that small amount of energy is required to form the activated complex, indicating that the product formation would be easier to achieve and thus bioenergy production through pyrolysis of MIW will be easier.

Further, the degree of stability of a system may be estimated by the value of change in Gibbs free energy (ΔG). The higher values indicate the harder reactivity and thus more energy will be absorbed by the system during the whole reaction process, and lower values indicate that the product can be produced with lower energy supply because of its reactive nature. Fig. 5d depicts the change in Gibbs free energy (ΔG_α) computed by DAE and Starink methods. In the present case, all ΔG_α values are positive indicating a non-spontaneous behavior of the pyrolytic process which consumes a considerable amount of energy to occur. The ΔG_α values varied with the conversion rate ($0.05 \leq \alpha \leq 0.7$), indicating that the system passed through ups and downs of the degree of difficulty [Fig. 5d; 0.05–0.1 (up), 0.1–0.15 (down), 0.15–0.2 (up), 0.2–0.4 (down), 0.4–0.65 (up), 0.65–0.7 (down)] for the MIW pyrolysis. The average values of ΔG were computed as 151.27 and 151.24 kJ mol^{-1} for DAE and Starink methods.

The entropy, being a state function, is an index to indicate degree of randomness or disorderness associated with the reaction system. The change of reaction entropy (ΔS_α) reflects how near the system is to its own thermodynamic equilibrium. The lower value of entropy (ΔS_α) signifies that the reactive system is approaching to its own thermodynamic equilibrium state. In this case, the substance shows low reactivity and thus, takes more reaction time to form the activated complex.[49] On the other hand, a large value of ΔS_α means the system is far from its thermodynamic equilibrium. In this case, the reactivity of material is high, and the reaction system will react faster to produce activated complex, and consequently, takes short reaction time to form the activated complex. For MIW pyrolysis, the ΔS_α values were found both positive as well as negative. The ΔS_α values were negative for each value of conversion (α) except α ranging from 0.3 to 0.5 (Fig. 5e).

Pyrolysis is a complex process and is governed by a set of parallel, complex and competitive reactions taking place simultaneously which involve the disintegration of natural polymers (hemicellulose, cellulose, and lignin) within the biomass material as well as integration of smaller molecules to form bigger molecules with the increase in temperature. The entropy of the system increases when bulky polymer molecules break to form a large number of volatiles/gas molecules and decrease when the smaller molecules combine to create a larger molecule during the pyrolysis process. The increment in ΔS_α values for conversion from 0.2 to 0.4 (311 to 338 °C) was largely due to the formation of a large number of molecules, owing to the simultaneous dissociation of hemicellulose, cellulose and lignin molecules.[50] The increment in ΔS_α values for above conversion range shows increase in reactivity which is supported by the fact that in this range ΔG_α values decrease monotonously indicating decrease in endothermicity of reaction. For, above conversion range, the increase in activation energy (E_α) and ΔH_α values show an increase in EB values as well as endothermicity of the reactive system. It is indicative of the fact that the system absorbs large amount of energy for dissociation of larger molecules in this range for which the entropy of the system has increased. After the above conversion range, the system entropy decreases up to a conversion value of 0.65 (384 °C), which is indicative of the association of small molecules to form product molecules within the reactive system.[44] This is consistent with the decrease in ΔH_α values that show a decrement in endothermicity of the reactive system. This supports the fact that in this region the entropy of the system decreases due to the dominance of reaction in which association of molecules takes place. In this range, EB slightly increases which is taken care of by the rising temperature.

For the conversion range ($0.05 \leq \alpha \leq 0.7$), the maximum negative value of ΔS_α was -23.06 J mol^{-1} K^{-1} for DAE method at $\alpha = 0.65$ and maximum positive value of 34.02 J mol^{-1} K^{-1} for Starink method at $a = 0.4$ (Table 6). This indicates that the system was in the highest state of stability at conversion value 0.65 ($T = 384$ °C) and most reactive around conversion value of 0.4 ($T = 338$ °C). It is interesting to see that the value of ΔG_α around conversion value 0.65 is also highest (Fig. 5d and Table 6) indicating that the endothermicity is very high and thus conducting reaction is difficult. Also around $\alpha = 0.4$, the A_α vs. α plot (Fig. 5a) showed the highest peaks, confirming that the system was most reactive around the conversion value at 0.4 which is also confirmed by DTG plot shown in Fig. 1b. For the rest of the conversion points, the negative value of ΔS_α reflects that activated complex needs comparatively more thermal energy to propagate the reaction in the forward direction or we can say that more or less the thermal equilibrium has been reached and a thermally stable product has been produced.[51] This statement are in accordance of the lower values of A_α as demonstrated in A_α vs. α plot (Fig. 5a), confirming the less reactivity of the system in the conversion range from $0.05 \leq \alpha < 0.3$ and further for $0.5 < \alpha \leq 0.7$.

The reaction rate constant (k) was computed using the Arrhenius correlation and found to be continuously increasing with conversion value up to 0.7 (Fig. 5f). The lowest and highest value of the rate constant for the pyrolysis of MIW was estimated to be ranged from 0.05 to 24.90 min^{-1}. It was expected as the temperature continuously increased in the range $0.05 \leq \alpha \leq 0.7$ and reaction rate constant is a strong function of temperature.

4 Conclusions

The following salient conclusions can be drawn from the present investigation:

1. The characterization for as-received MIW revealed high volatile content, fixed carbon, and higher heating value as 73.38 mass%, 15.09 mass%, and 14.89 MJ kg^{-1}, respectively. Further, no sulfur was detected in MIW sawdust.

2. There was no major discrepancy in apparent activation energy values computed by DAE (154.86 kJ mol^{-1}) and Starink (155.74 kJ mol^{-1}) methods.

3. The reaction mechanism for the pyrolysis of MIW can be classified as one-dimensional diffusion type (D$_1$; $g(\alpha) = \alpha^2$) for 5–50% conversion followed by five and a half order (F$_{5.5}$; $g(\alpha) = [1 - 1/(1 - \alpha)^{4.5}]/-4.5$) heterogeneous rate expression up to the rest conversion value of 70%.

4. The average values of A, ΔH and ΔG obtained were 2.2 × 10^{14} min^{-1}, 149.79 kJ mol^{-1} and 151.27 kJ mol^{-1} for DAE method and 2.6 × 10^{14} min^{-1}, 150.67 kJ mol^{-1} and 151.24 kJ mol^{-1} for Starink method, respectively.

Nomenclature

α	Conversion or reaction progress, dimensionless
β	Heating rate, °C min^{-1}
E_a	Apparent activation energy, kJ mol^{-1}
E_α	Activation energy at conversion α, kJ mol^{-1}
A	Frequency factor, min^{-1}
k	Reaction rate constant, min^{-1}
n	Order of reaction, dimensionless
R	Universal gas constant, kJ mol^{-1} K^{-1}
T	Temperature, K in all equations and °C elsewhere
$p(x)$	Exponential/temperature integral approximation
$f(\alpha)$	Differential form of reaction model
$g(\alpha)$	Integral form of reaction model
R^2	Correlation coefficient, dimensionless

Abbreviations

MIW	*Mangifera indica* wood
TG	Thermogravimetric analysis/thermogravimetry
DTG	Derivative thermogravimetry
DAE	Distributed activation energy
C–R	Coats–Redfern
ASTM	American Society for Testing and Materials
HHV	Higher heating value or gross calorific value
LHV	Lower heating value or net calorific value
EB	Energy barrier

Conflicts of interest

There are no conflicts to declare.

Acknowledgements

References

1 M. Parikka, *Biomass Bioenergy*, 2004, **27**, 613–620.
2 A. Sharma and B. Mohanty, *Int. J. Energy Res.*, 2021, 1–15.
3 S. Shrivastava and A. K. Saxena, *Wood is good: But, is India doing enough to meet its present and future needs?* Centre for Science and Environment, New Delhi, 2017.
4 B. Ling, J. Tang, F. Kong, E. J. Mitcham and S. Wang, *Food Bioprocess Technol.*, 2015, **8**, 343–358.
5 S. Vyazovkin and N. Sbirrazzuoli, *Macromol. Rapid Commun.*, 2006, **27**, 1515–1532.
6 M. Labus and I. Matyasik, *J. Therm. Anal. Calorim.*, 2019, **136**, 1185–1194.
7 B. Saha, A. K. Maiti and A. K. Ghoshal, *Thermochim. Acta*, 2006, **444**, 46–52.
8 E. Müsellim, M. H. Tahir, M. S. Ahmad and S. Ceylan, *Appl. Therm. Eng.*, 2018, **137**, 54–61.
9 X. Xu, R. Pan, P. Li and R. Chen, *Appl. Biochem. Biotechnol.*, 2020, **191**, 1605–1623.
10 S. A. Channiwala and P. P. Parikh, *Fuel*, 2002, **81**, 1051–1063.
11 P. Basu, *Biomass gasification and pyrolysis, practical design and theory*, 2010.
12 S. Li, S. Xu, S. Liu, C. Yang and Q. Lu, *Fuel Process. Technol.*, 2004, **85**, 1201–1211.
13 A. Sharma and B. Mohanty, *Energy Sources, Part A*, 2020, **42**, 1–18.
14 O. Bianchi, J. D. N. Martins, R. Fiorio, R. V. B. Oliveira and L. B. Canto, *Polym. Test.*, 2011, **30**, 616–624.
15 J. Li, C. Zhang, R. Yin and W. Zhang, *RSC Adv.*, 2019, **9**, 8415–8425.
16 M. J. Starink, *Thermochim. Acta*, 2003, **404**, 163–176.
17 A. W. Coats and J. P. Redfern, *Nature*, 1964, **201**, 68–69.
18 A. Khawam and D. R. Flanagan, *J. Phys. Chem. B*, 2006, **110**, 17315–17328.
19 J. M. Criado, J. Málek and A. Ortega, *Thermochim. Acta*, 1989, **147**, 377–385.
20 L. Núñez, F. Fraga, M. R. Núñez and M. Villanueva, *Polymer*, 2000, **41**, 4635–4641.
21 M. U. H. Joardder, M. S. Uddin and M. N. Islam, *Adv. Mech. Eng.*, 2011, **2012**, 316806.
22 K. Parmar, *IRA Int. J. Appl. Sci.*, 2017, **7**, 42.
23 B. Cagnon, X. Py, A. Guillot, F. Stoeckli and G. Chambat, *Bioresour. Technol.*, 2009, **100**, 292–298.
24 J. Zhang, T. Chen, J. Wu and J. Wu, *RSC Adv.*, 2014, **4**, 17513–17520.
25 J. J. A. Flores, J. G. R. Quiñones, M. L. Á. Rodríguez, J. V. A. Vera, J. E. Valencia, S. J. G. Martínez, F. M. Montesino and A. A. Rosas, *Energies*, 2020, **13**, 969.
26 K. Slopiecka, P. Bartocci and F. Fantozzi, *Appl. Energy*, 2012, **97**, 491–497.

27 Z. Chen, Q. Zhu, X. Wang, B. Xiao and S. Liu, *Energy Convers. Manage.*, 2015, **105**, 251–259.

28 A. Soria-Verdugo, M. T. Morgano, H. Mätzing, E. Goos, H. Leibold, D. Merz, U. Riedel and D. Stapf, *Energy Convers. Manage.*, 2020, **212**, 112818.

29 R. K. Mishra and K. Mohanty, *Bioresour. Technol.*, 2018, **251**, 63–74.

30 A. Sharma and B. Mohanty, *J. Therm. Anal. Calorim.*, 2020, **141**, 1–15.

31 X. Xu, R. Chen, R. Pan and D. Zhang, *Energy Fuels*, 2020, **34**, 1859–1869.

32 P. Ghodke and R. N. Mandapati, *Fuel*, 2019, **236**, 1008–1017.

33 A. K. Varma and P. Mondal, *Energy Sources, Part A*, 2016, **38**, 2536–2544.

34 A. Garcia-Maraver, J. A. Perez-Jimenez, F. Serrano-Bernardo and M. Zamorano, *Renewable Energy*, 2015, **83**, 897–904.

35 H. Alhumade, J. C. G. da Silva, M. S. Ahmad, G. Çakman, A. Yıldız, S. Ceylan and A. Elkamel, *J. Anal. Appl. Pyrolysis*, 2019, **140**, 385–392.

36 X. Zhang, W. Yang and W. Blasiak, *Energy Fuels*, 2011, 4786–4795.

37 J. Zhang, Y. S. Choi and C. G. Yoo, *ACS Sustainable Chem. Eng.*, 2015, **3**, 293–301.

38 F. X. Collard and J. Blin, *Renewable Sustainable Energy Rev.*, 2014, **38**, 594–608.

39 K. Werner, L. Pommer and M. Broström, *J. Anal. Appl. Pyrolysis*, 2014, **110**, 130–137.

40 A. Chandrasekaran, S. Ramachandran and S. Subbiah, *Bioresour. Technol.*, 2017, **233**, 413–422.

41 Z. Ma, D. Chen, J. Gu, B. Bao and Q. Zhang, *Energy Convers. Manage.*, 2015, **89**, 251–259.

42 H. Cai, J. Liu, W. Xie, J. Kuo, M. Buyukada and F. Evrendilek, *Energy Convers. Manage.*, 2019, **184**, 436–447.

43 M. Poletto, A. J. Zattera and R. M. C. Santana, *Bioresour. Technol.*, 2012, **126**, 7–12.

44 Y. F. Chang, *NeuroQuantology*, 2013, **11**, 189–196.

45 X. Yuan, T. He, H. Cao and Q. Yuan, *Renewable Energy*, 2017, **107**, 489–496.

46 R. Kaur, P. Gera, M. K. Jha and T. Bhaskar, *Bioresour. Technol.*, 2018, **250**, 422–428.

47 R. K. Singh, T. Patil and A. N. Sawarkar, *Bioresour. Technol. Rep.*, 2020, **12**, 100558.

48 L. T. Vlaev, V. G. Georgieva and S. D. Genieva, *J. Therm. Anal. Calorim.*, 2007, **88**, 805–812.

49 R. Kaur, P. Gera, M. K. Jha and T. Bhaskar, *Bioresour. Technol.*, 2018, **250**, 422–428.

50 H. Yang, R. Yan, H. Chen, D. H. Lee and C. Zheng, *Fuel*, 2007, **86**, 1781–1788.

51 A. Shahid, M. Ishfaq, M. S. Ahmad, S. Malik, M. Farooq, Z. Hui, A. H. Batawi, M. E. Shafi, A. A. Aloqbi, M. Gull and M. A. Mehmood, *Bioresour. Technol.*, 2019, **289**, 121701.